Journal of Alloys and Compounds 513 (2012) 359–364

Contents lists available at SciVerse ScienceDirect

Journal of Alloys and Compounds

journal homepage: www.elsevier.com/locate/jallcom

Photocatalytic activity of mixture of ZrO_2/SnO_2, ZrO_2/CeO_2 and SnO_2/CeO_2 nanoparticles

H.R. Pouretedal[a,*], Z. Tofangsazi[b], M.H. Keshavarz[a]

[a] Faculty of Applied Chemistry, Malek-ashtar University of Technology, Shahin-Shahr, Iran
[b] Department of Chemistry, Islamic Azad University, Shahreza Branch, Shahreza, Iran

ARTICLE INFO

Article history:
Received 23 August 2011
Accepted 18 October 2011
Available online 25 October 2011

Keywords:
Photocatalyst
ZrO_2
SnO_2
CeO_2
Nanoparticles

ABSTRACT

The ZrO_2, SnO_2 and CeO_2 nanoparticles synthesized by sol–gel procedure and calcined at 550 °C. The prepared nanoparticles characterized by X-ray diffraction spectroscopy, transmission electron microscopy and IR spectrophotometry. The structure of prepared nanoparticles were tetragonal and monoclinic as confirmed from the XRD patterns. The photocatalytic activity of ZrO_2, SnO_2, CeO_2 nanoparticles and the mixture of 1:1 of ZrO_2/SnO_2, ZrO_2/CeO_2 and SnO_2/CeO_2 studied in 2-nitrophenol degradation reaction. The order of photocatalytic activity is $ZrO_2/SnO_2 > ZrO_2/CeO_2 > SnO_2/CeO_2 > ZrO_2 > SnO_2 > CeO_2$. Among mixtures of ZrO_2/SnO_2, the mixture with weight ratio of 4:1 showed the highest photocatalytic activity. The results indicated the ZrO_2 nanoparticles with the more band-gap energy had an important role in photocatalytic activity. The mixture of ZrO_2/SnO_2 (4:1) is also indicated the higher photocatalytic activity in comparison to $Zr_{0.8}Sn_{0.2}O_2$ nanocomposite. The complete degradation of 2-nitrophenol was obtained at time 45 min in the presence of hydrogen peroxide (0.1 g/L) and the mixture of ZrO_2/SnO_2 (4:1).

1. Introduction

The degradation of organic pollutants in water and air by photocatalysis, using semiconductors, such as TiO_2, CeO_2, ZrO_2, SnO_2 and so on, has attracted extensive attention during recent 20 years [1]. The use of semiconductors as photocatalyst in photodegradation process is a technique to increase the rate of process. The semiconductors can increase the degradation of most kinds of persistent organic pollutants, such as detergents, dyes, pesticides and volatile organic compounds, under UV-light irradiation [2–5]. However, the fast recombination rate of photogenerated electron/hole pairs hinders the commercialization of this technology [1]. Thus, it is of great interest to improve the photocatalytic activity of semiconductors for the degradation process [5,6]. The synthesis of different photocatalysts with various compositions and the use of photocatalysts in various conditions can be an attractive field of researches [7,8]. Mixed oxide composite materials can often be more efficient photocatalysts than pure substances. This phenomenon arises through the generation of new active sites due to interactions between two oxides as substrate and dopant, through improved mechanical strength, thermal stability, and surface area of doped substrate [5,6].

Zirconium oxide is an *n*-type semiconductor with band-gap energy of 5.0 eV that used as heterogeneous catalyst. The values range of band-gap is reported between 3.25 and 5.1 eV depending on the preparation technique of the sample and the most frequent and accepted value is 5.0 eV. The conductance and valence band potentials of it is −1.0 and +4.0 V versus NHE, respectively, allowing its use as a photocatalyst in the production of hydrogen through water decomposition [9,10]. Although ZrO_2 presents an adsorption maximum around 250 nm, some samples show a non-negligible absorption in the near UV range (290–390 nm) and photocatalytic reactions could be performed under irradiation in this range [10]. Cerium (IV) oxide nanoparticles (as an *n*-type semiconductor with a much narrower band-gap of 3.3 eV) have received much attention because of its many interesting characteristics, such as unique UV absorption ability, high stability at high temperature, high hardness and reactivity [11]. Thus, CeO_2 and CeO_2-based materials have been extensively used in a wide variety of applications such as solid oxide fuel cells (SOFCs), catalysis, luminescent materials, gas sensors, polishing materials, and ferromagnetic oxides and so on [12]. SnO_2 is a semiconductor with band-gap energy of about 3.65 eV at bulk state and is an *n*-type semiconductor crystallizing in tetragonal rutile structure. SnO_2 has been reported as a suitable gas sensing oxide and recently its composites have been studied as promising semiconductors in the photocatalytic degradation of wastewaters [13]. Tin (IV) oxide has been a widely studied material because of its wide range of applications as gas sensors, heat mirrors, and transparent electrodes for solar cells, opto-electronic devices and in catalysis [14].

Photocatalytic reaction is initiated when a photoexcited electron is promoted from the filled valence band of semiconductor

* Corresponding author. Tel.: +98 312 5912253; fax: +98 312 5220420.
E-mail address: HR_POURETEDAL@mut-es.ac.ir (H.R. Pouretedal).

0925-8388/$ – see front matter © 2011 Elsevier B.V. All rights reserved.
doi:10.1016/j.jallcom.2011.10.049

photocatalyst (SC) to the empty conduction band as the absorbed photon energy, $h\nu$, equals or exceeds the band-gap of the semiconductor photocatalyst leaving behind a hole in the valence band. Thus in concert, electron and hole pair (e^-–h^+) is generated. The following chain reactions have been widely postulated [1,7,8].

$$\text{Photoexcitation}: MO_2/SC + h\nu \rightarrow e^- + h^+ \quad M: Zr, Ce, Sn \tag{1}$$

$$\text{Oxygen ionosorption}: (O_2)_{ads} + e^- \rightarrow O_2^{\bullet -} \tag{2}$$

$$\text{Ionization of water}: H_2O \rightarrow OH^- + H^+ \tag{3}$$

$$\text{Protonation of superoxides}: O_2^{\bullet -} + H^+ \rightarrow HOO^{\bullet} \tag{4}$$

The hydroperoxyl radical formed (Eq. (4)) also has scavenging property as O_2 thus doubly prolonging the lifetime of photohole:

$$HOO^{\bullet} + e^- \rightarrow HO_2^- \tag{5}$$

$$HOO^- + H^+ \rightarrow H_2O_2 \tag{6}$$

Both the oxidation and reduction can take place at the surface of the photoexcited semiconductor photocatalyst. Recombination between electron and hole occurs unless oxygen is available to scavenge the electrons to form superoxides ($O_2^{\bullet -}$), its protonated form the hydroperoxyl radical ($HO_2^{\bullet}$) and subsequently H_2O_2 [15,16].

In the light of the literature studies, this study was designed to synthesis nanoparticles of ZrO_2, CeO_2 and SnO_2 by sol–gel procedure. The different composition of prepared nanoparticles was used in 2-nitrophenol photodegradation.

2. Experimental

2.1. Synthesis of nanoprticles

The sol–gel method used to prepare of ZrO_2, CeO_2 and SnO_2 nanoparticles. The ammonium cerium (IV) nitrate ($(NH_4)_2Ce(NO_3)_6$, Merck), zirconium oxychloride ($ZrOCl_2{\cdot}8H_2O$, Merck) and tin (IV) chloride ($SnCl_4{\cdot}5H_2O$, Merck) used as starting materials to prepare CeO_2, ZrO_2 and SnO_2 nanoparticles, respectively. The 0.1 M solutions of Ce(IV), Zr(IV) and Sn(IV) prepared and the nitric acid diluted solution added drop by drop until these solutions became clear. Deionized and double distilled water used to prepare the solutions. The solutions aged overnight and are called "sol". Next, the ammonia solution (1:1) added drop by drop until the gel samples obtained at pH of 7–8. The gel samples aged overnight. After aging, the gel samples of $Ce(OH)_4$, $Zr(OH)_4$ and $Sn(OH)_4$ dried at 100 °C for 2 h and followed by calcined at 550 °C for 3 h. The light yellowish CeO_2, white ZrO_2 and white SnO_2 nanoparticles obtained after calcinations process and then stored for further use.

2.2. Characterization of nanoparticles

IR-spectra of ZrO_2, CeO_2 and SnO_2 nanoparticles in range 4000–400 cm^{-1} recorded by using Nicolet Impact 400D FT-IR Spectrophotometer. A diffractometer Bruker D8 ADVANCE Germany with anode of Cu ($\lambda = 1.5406$ Å of Cu K_α) and filter of Ni applied to record of X-ray diffraction (XRD) patterns of nanoparticles. A JEOL JEM-1200EXII transmission electron microscope (TEM) operating at 120 kV use for estimation of nanoparticles size. The supporting grids were formvar-covered, carbon-coated, 200-mesh copper grids. BET (Brunauer–Emmett–Teller) surface area of nanoparticles determined by using Monosorb Quantochorom.

2.3. Photocatalytic activity of nanoprticles

The photocatalytic activity of prepared nanoprticles studied in photodegradation of 2-nitrophenol. Phenol and its derivatives such as 2-nitrophenol are industrially important chemicals and thus their presence in the environment is relatively very common. Due to their high toxicity, they represent a group of dangerous chemicals even at low concentrations [17].

Photodegradation experiments perform in a photocatalytic reactor system. A 70 W mercury low pressure lamp uses as irradiation source. The lamp and the tube immersed in the photoreactor cell with a light path of 3.0 cm. The photoreactor filled with 50 ml of 10–50 mg/L of 2-nitrophenol and 0.1–0.8 g/L of photocatalysts. The ZrO_2, CeO_2, SnO_2 and mixture of ZrO_2/CeO_2, ZrO_2/SnO_2 and CeO_2/SnO_2 use as photocatalysts. The whole reactor cooled with a water-cooled jacket on its outside and the temperature was kept at 25 °C. All reactants in the reactions stir using a magnetic stirrer for ensure that the suspension of the catalyst was uniform during the course of the reaction. In order to setting the adsorption/desorption equilibrium of 2-nitrophenol on heterogeneous catalysts surface, the reactor keep in dark conditions within 30 min.

The degradation efficiency of 2-nitrophenol determined with measurement of absorbance of samples by a UV–vis spectrophotometer Carry-100 using a paired 1.0 cm quartz cell. The samples centrifuged to remove the nanoparticles before absorbance measurement. The absorbance of samples before (A_o) and after a distinct time (A_t) of irradiation and Beers' law to determination of C_o and C_t use for calculate of degradation efficiency (Eq. (7)).

$$\%\text{Degradation} = 100 \times \left[1 - \frac{C_t}{C_o}\right] = 100 \times \left[1 - \frac{A_t}{A_o}\right] \tag{7}$$

The pH of samples, the dosage of catalysts and the presence of hydrogen peroxide investigated on the reactivity of photocatalysts. The hydrochloric acid and sodium hydroxide (0.01 M) and a Metrohm pH-meter with combined electrode used to control of samples pH at range of 3–9.

3. Results and discussion

3.1. Characterization of nanoparticles

The X-ray diffraction patterns of SnO_2, ZrO_2 and CeO_2 nanoparticles calcined at temperature of 550 °C are indicated in Fig. 1A–C, respectively. As seen from Fig. 1A, the diffraction peaks of (1 1 0), (1 0 1), (2 1 1) and (1 1 2) at 2θ of 26.8, 34.0, 51.8 and 64.8°, respectively, show the formation of Cassiterite type tetragonal crystals of SnO_2 which matches well with JCPDS card # 41-1445 [18]. The average of crystalline size (D_T) is calculated 3.5 nm from the $(1\,1\,0)_T$ diffraction peak using Scherrer's equation (Eq. (8)) [19].

$$D_T = \frac{(0.9\lambda)}{(\beta \cos\theta)} \tag{8}$$

In Eq. (8), D is the average crystalline size in nm, λ is the radiation wavelength (0.154 nm), β is the corrected half-width at half-intensity and θ is the diffraction peak angle.

Zirconium dioxide is one of the most studied semiconductor materials. Pure ZrO_2 has a monoclinic crystal structure at room temperature and transitions to tetragonal and cubic at increasing temperatures [20]. The formation of crystalline forms of tetragonal and monoclinic observes for ZrO_2 nanoparticles calcined at temperature 550 °C (Fig. 1B). The tetragonal structure of ZrO_2 can be considered as the distortion of the cubic structure of ZrO_2 and its adjacent diffraction-peak pairs ((0 0 2), (1 1 0)) at 34°, ((1 1 2), (2 0 0)) at 50°, and ((1 0 3), (2 1 1)) at 60° (2θ), which originate from the splitting of the cubic diffraction peaks of (2 0 0), (2 2 0) and (3 1 1) [21,22]. The average crystallite size of ZrO_2 crystal is calculated from Debye–Scherrer formula [19] and found 12.3 nm.

Fig. 1C show the XRD pattern of nanosized CeO_2 powder in 2θ of 20–80°. The five peaks with 2θ values of 28.6°, 33.2°, 47.5°, 56.4° and 59.2° correspond to the (1 1 1), (2 0 0), (2 2 0), (3 1 1) and (2 2 2) planes indicate the formation of pure-phase CeO_2 in a cubic fluorite structure [23,24]. It is clear that all Bragg reflections for sample agree well with those of standard CeO_2 and noticeably broadened of all reflections show the fine nature of CeO_2 particles. The size of CeO_2 particles is obtained 8.2 nm by Debye–Scherrer formula.

The transmission electron microscopy images of SnO_2, ZrO_2 and CeO_2 nanoparticles are shown in Fig. 2A–C, respectively. The spherical topography saw from the TEM images for prepared nanoparticles. The formation of nanoparticles with size less than 20 nm confirmed by TEM images that agreement with results of XRD analysis. The TEM analysis also shows a slightly irregular and rounded shape for synthesized nanoparticles. The IR spectra of prepared nanoparticles of SnO_2, ZrO_2 and CeO_2 showed an absorption band at range of 500–450 cm^{-1} that is related to the vibration of M–O–M bond in MO_2 with M: Sn, Zr and Ce [25,26]. BET (Brunauer–Emmett–Teller) surface area of prepared photocatalysts determined by using Monosorb Quantochorom and obtained 263.4, 254.6 and 231.8 m^2/g for SnO_2, ZrO_2 and CeO_2, respectively.

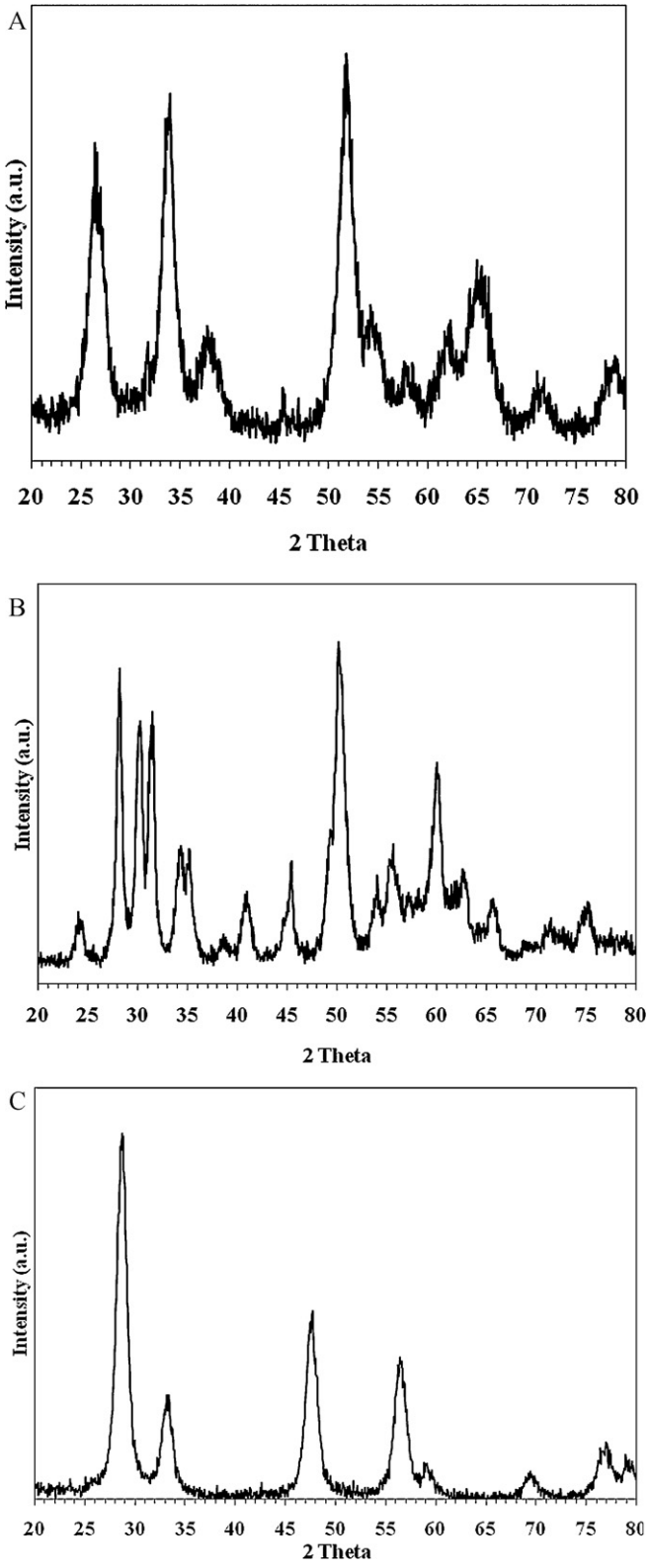

Fig. 1. (A) XRD pattern of SnO_2 nanoparticles. (B) XRD pattern of ZrO_2 nanoparticles. (C) XRD pattern of CeO_2 nanoparticles.

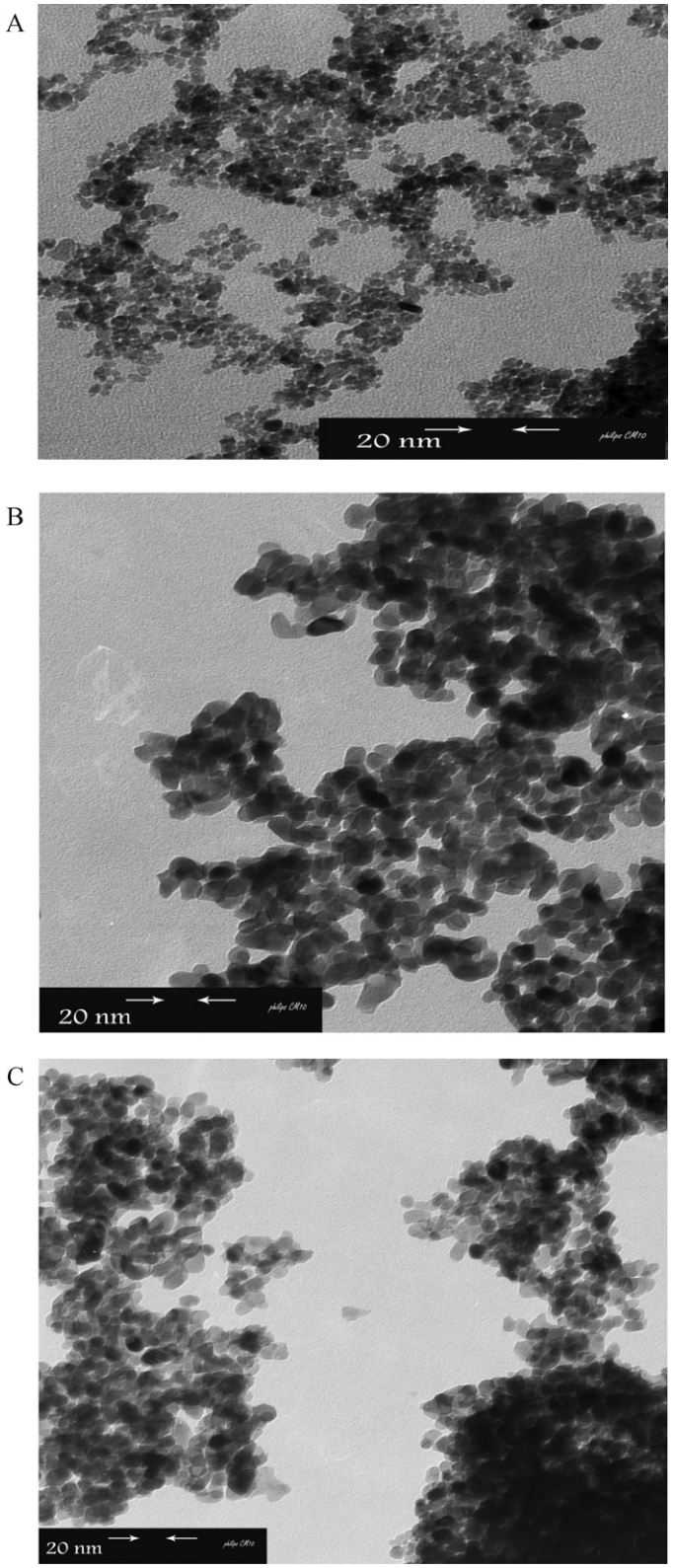

Fig. 2. (A) TEM image of SnO_2 nanoparticles. (B) TEM image of ZrO_2 nanoparticles. (C) TEM image of CeO_2 nanoparticles.

3.2. Photocatalytic activity of nanoparticles

The photodegradation of 2-nitrophenol (20 mg/L) catalyzed by prepared nanoparticles (0.1 g/L) at different pHs and in duration of 4 h is shown in Figs. 3 and 4. The reactor is containing 0.05 g/L of each photocatalyst and thus the total amount of 0.1 g/L of mixture of nanoparticles. As seen from Figs. 3 and 4, the highest degradation for 2-nitrophenol obtained at pH of 5. The isoelectric points (IEP) of metal oxide influence on the charge of their surfaces. The metal oxides of ZrO_2, CeO_2 and SnO_2 are as colloids or larger particles

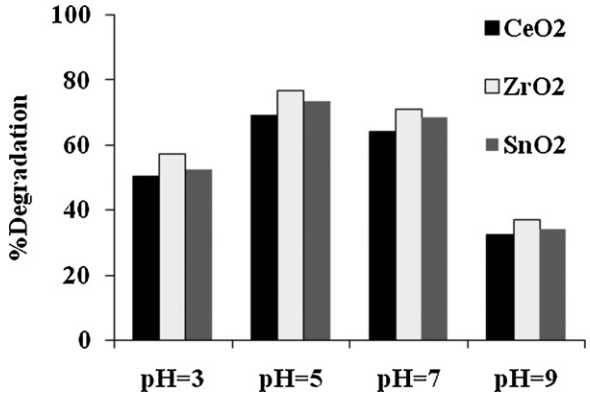

Fig. 3. Dgradation efficiency of 2-nitrophenol (20 mg/L) catalyzed by nanoparticles (0.1 g/L) in duration of 4 h.

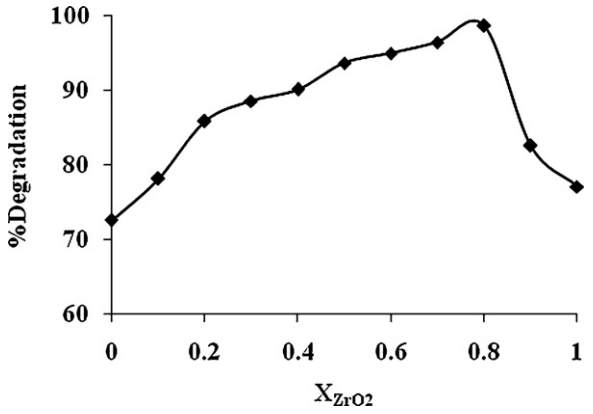

Fig. 5. The effect of weight fraction of ZrO_2 in mixture of SnO_2/ZrO_2 on the dgradation efficiency of 2-nitrophenol.

in aqueous solution. The surface of them is generally assumed to be covered with surface hydroxyl species of M–OH. At pH values above the IEP, the predominate surface species is $M–O^-$, while at pH values below the IEP, $M–OH_2^+$ species predominate [8]. The IEP of ZrO_2, CeO_2 and SnO_2 is at pH of 4–7 [27]. Thus, the charge of catalysts is positive in pH < 7 and negative in pH > 7. In pH of 5, the 2-nitrophenol molecules are neutral and maximum absorption of their occur on the surface of catalysts. In pH values over 7, the repulsive of phenolate ions with negative charge of surface of catalysts due to a considerable reduction of degradation efficiency.

The order of photocatalytic activity of catalysts is $SnO_2/ZrO_2 > CeO_2/ZrO_2 > SnO_2/CeO_2 > ZrO_2 > SnO_2 > CeO_2$. Zirconium oxide is an *n*-type semiconductor with band-gap energy of 5.0 eV. Apparently, the more band-gap energy of ZrO_2 versus CeO_2 and SnO_2 (3.3–3.7 eV) is due to an increasing of lifetime of photogenerated electrons and holes and decrease of recombination rate of them [16,8]. Thus, the mixtures contain ZrO_2 include SnO_2/ZrO_2 and CeO_2/ZrO_2 show the more activity versus SnO_2/CeO_2 mixture.

Fig. 5 shows the effect of weight fraction of ZrO_2 in mixture of SnO_2/ZrO_2 (total amount of 0.1 g/L) on the photocatalytic activity of it in 2-nitrophenol degradation. As seen, the highest reactivity is obtained for mixture of SnO_2/ZrO_2 with $x_{ZrO_2} = 0.8$. As the other words, a mixture of SnO_2/ZrO_2 with weight ratio of 1:4 show the most degradation for 2-nitrophenol. Also, increasing of total amount of mixture of photocatalyst up to 0.5 g/L is due to increasing of rate of degradation. However, the weight ratio of SnO_2/ZrO_2 is 1:4. But, the loading of 0.5 g/L show a reduction in degradation efficiency. The degradation efficiencies in duration 3 h obtained 56.4, 62.7, 69.8 and 66.2 for the dosage of 0.1, 0.3, 0.5 and 0.8 g/L, respectively. The decrease in photodegradation efficiency beyond 0.5 g/L of mixture of photocatalysts may be attributed to the screening effect of excess heterogeneous particles in the solution and scattering of light [28,29].

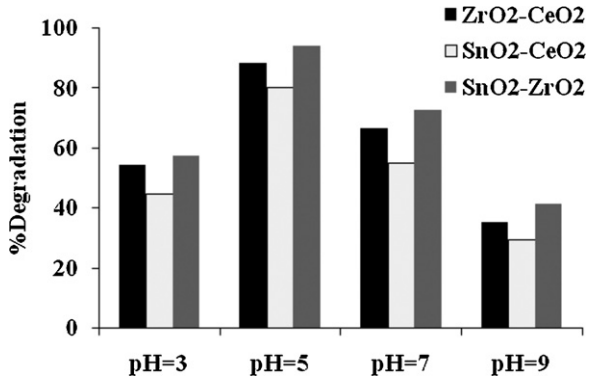

Fig. 4. Dgradation efficiency of 2-nitrophenol (20 mg/L) catalyzed by mixture of nanoparticles (0.1 g/L) in duration of 4 h.

3.3. The kinetic of photodegradation

The degradation experiments for UV–vis irradiation of 2-nitrophenol aqueous solutions containing mixture of SnO_2/ZrO_2 (1:4) follow first-order kinetics with respect to the concentration of the pollutant in the bulk solution (C) [30,31]:

$$r = \frac{-dC}{dt} = k_{app}C \tag{9}$$

in which k_{app} is the apparent first-order rate constant (with the same restriction of $C = C_o$ at $t = 0$, with C_o being the initial content in the bulk solution after dark adsorption and t the reaction time), and is affected by 2-nitrophenol concentration. Integration of this equation will lead to the expected relation:

$$\ln\left(\frac{C_o}{C}\right) = k_{app}t \tag{10}$$

The values of k_{app} can be obtained directly from the regression analysis the linear curve of plot of $\ln(C_o/C)$ versus t. The results are indicated in Table 1.

3.4. Synthesis of $Sn_{0.2}Zr_{0.8}O_2$ composite

In order to study of circumstance of catalyst on the photoactivity of it, $Sn_{0.2}Zr_{0.8}O_2$ composite prepared. The solution of Sn^{4+} and Zr^{4+} with mole ratio of 1:4 used as starting materials. After aging, the composite gel of $Sn_{0.2}Zr_{0.8}O_2$ dried at 100 °C for 2 h and then calcined at 550 °C for 3 h. The XRD pattern and TEM image of $Sn_{0.2}Zr_{0.8}O_2$ composite are shown in Fig. 6A and B, respectively. The tetragonal structure of composite with particles size of less than 20 nm confirmed by XRD pattern and TEM image. The tetragonal phase of composite proved with JCPDS card # 37-1413 and

Table 1
The apparent rate constants (k_{app}, h^{-1}) and regression coefficients (R^2) of 2-nitrophenol degradation catalyzed by nanoparticles of mixture of SnO_2/ZrO_2 (1:4) and composite of $Sn_{0.2}Zr_{0.8}O_2$.

C_o, mg/L	mixture of SnO_2/ZrO_2 (1:4)		composite of $Sn_{0.2}Zr_{0.8}O_2$	
	k_{app}	R^2	k_{app}	R^2
10	1.283	0.924	0.345	0.950
20	1.040	0.955	0.314	0.981
30	0.685	0.973	0.272	0.983
40	0.518	0.963	0.186	0.989
50	0.390	0.959	0.160	0.997

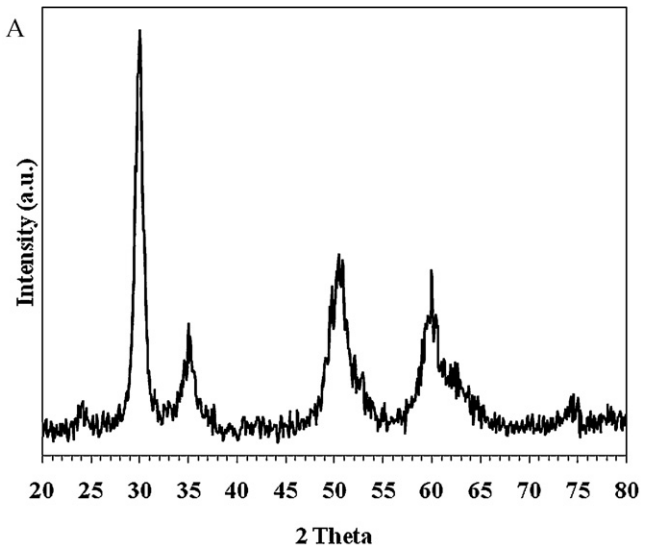

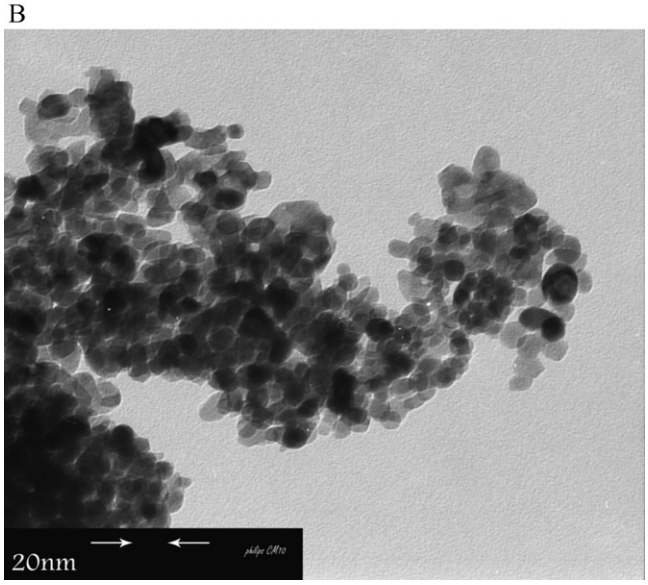

Fig. 6. (A) XRD pattern of $Sn_{0.2}Zr_{0.8}O_2$ composite. (B) TEM image of $Sn_{0.2}Zr_{0.8}O_2$ composite.

29-1484 for ZrO_2 and SnO_2, respectively [21,32]. The composition of composite obtained 78.8% of ZrO_2 and 21.2% of SnO_2 by XRD analysis that show the structure of composite is $Sn_{0.21}Zr_{0.79}O_2$. BET (Brunauer–Emmett–Teller) surface area of $Sn_{0.2}Zr_{0.8}O_2$ nanocomposite obtained 241.3 m^2/g.

The apparent first-order rate constant of 2-nitrophenol degradation catalyzed by $Sn_{0.2}Zr_{0.8}O_2$ composite are collected in Table 1. The obtained results show the more activity of mixture of SnO_2/ZrO_2 (1:4) versus composite of $Sn_{0.2}Zr_{0.8}O_2$ as photocatalyst in photodegradation reaction of 2-nitrophenol.

3.5. The reusability

The reusability of mixture of SnO_2/ZrO_2 (1:4) in photocatalytic activity examined in five-cycles. In the end of each cycle, the catalyst removed, washed and dried at 80 °C at time of 2 h and reused in following cycle. The results are indicated in Fig. 7. The degradation of 50% in fifteen-cycle indicates the performance of mixture of SnO_2/ZrO_2 (1:4) as photocatalyst.

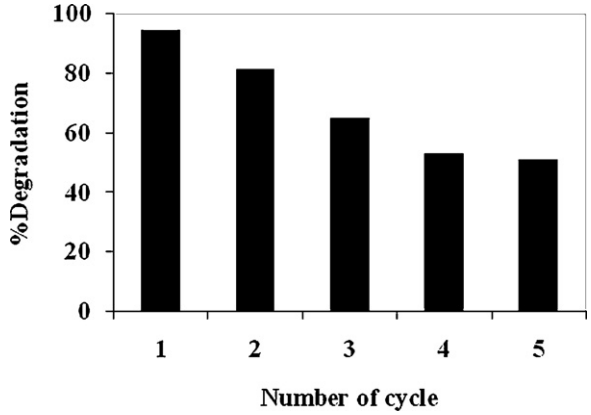

Fig. 7. The reusability of mixture of SnO_2/ZrO_2 (1:4) as photocatalyst in degradation of 2-nitrophenol.

3.6. The effect of H_2O_2

As seen from results, the complete degradation of 2-nitrophenol obtained at time 4 h. In order to reduction of time of degradation, the hydrogen peroxide as an oxidant added to the reactor. A degradation of more than 99% is seen at presence of 0.1 g/L of H_2O_2 and 0.5 g/L of mixture of SnO_2/ZrO_2 (1:4) duration of 45 min. Also, the k_{app} value for 2-nitrophenol (20 mg/L) degradation calculated 0.178 min^{-1}. The concentration of $OH^\bullet$ radical increase in the presence of H_2O_2 because it inhibit the electron–hole recombination according to the Eq. (11) [33].

$$MO_2(e^-) + H_2O_2 \rightarrow MO_2 + OH^- + OH^\bullet \quad (11)$$

Also, the electrons in conduction band can be adsorbed by H_2O_2 and thus the charge separation promoted in semiconductor. On the other hand, H_2O_2 forms hydroxyl radical according the Eqs. (12) and (13) [34].

$$H_2O_2 + e^- \rightarrow OH^- + OH^\bullet \quad (12)$$

$$H_2O_2 + O_2{}^{-\bullet} \rightarrow OH^- + OH^\bullet + O_2 \quad (13)$$

Thus, the rate of degradation of a pollutant can considerably increase with presence hydrogen peroxide beside of a photocatalyst.

4. Conclusion

The sol–gel procedure used to prepare of ZrO_2, CeO_2 and SnO_2 nanoparticles. The use of mixture of photocatalysts improved the activity of catalysts and therefore the rate of photodegradation of 2-nitrophenol. The composition of mixture as well as pH of samples influenced on the reactivity of catalysts. So that, the mixture of ZrO_2/SnO_2 with weight ratio of 4:1 and total amount of 0.5 g/L in pH 5 showed the highest activity. The performance of nanoparticles mixture of ZrO_2/SnO_2 as catalyst was more than nanocomposite of $Sn_{0.2}Zr_{0.8}O_2$.

References

[1] M.R. Hoffmann, S.T. Martin, W.Y. Choi, D.W. Bahnemann, Chem. Rev. 95 (1995) 69–96.
[2] P. Qu, J.C. Zhao, T. Shen, H. Hidaka, J. Mol. Catal. A: Chem. 129 (1998) 257–268.
[3] P. Peralta-Zamora, S.G. de Moraes, R. Pelegrini, M. Freire Jr., J. Reyes, H. Mansilla, N. Duran, Chemosphere 36 (1998) 2119–2133.
[4] A.L. Linsebigler, G.Q. Lu, J.T. Yates Jr., Chem. Rev. 95 (1995) 735–758.
[5] W. Cun, Z. Jincai, W. Xinming, M. Bixian, S. Guoying, P. Ping'an, F. Jiamo, Appl. Catal. B 39 (2002) 269–279.
[6] M.E. Manrĩquez, T. Lĩopez, R. Gĩ omez, J. Navarrete, J. Mol. Catal. A 220 (2004) 229–237.
[7] U.I. Gaya, A.H. Abdullah, J. Photochem. Photobiol. C 9 (2008) 1–12.

[8] K. Rajeshwar, M.E. Osugi, W. Chanmanee, C.R. Chenthamarakshan, M.V.B. Zanoni, P. Kajitvichyanukul, R. Krishnan-Ayer, J. Photochem. Photobiol. C 9 (2008) 171–192.
[9] C. Karunakaran, S. Senthilvelan, J. Mol. Catal. A 233 (2005) 1–8.
[10] N. Smirnova, Y. Gnatyuk, A. Eremenko, G. Kolbasov, V. Vorobetz, I. Kolbasova, O. Linyucheva, Int. J. Photoenergy (2006) 1–6, Article ID 85469.
[11] S. Phoka, P. Laokul, E. Swatsitang, V. Promarak, S. Seraphin, S. Maensiri, Mater. Chem. Phys. 115 (2009) 423–428.
[12] X.Y. Li, W.F. Chen, X.Z. Zhou, Z.Y. Gu, C.M. Chen, Mater. Lett. 59 (2005) 48–52.
[13] S.R. Dhage, S.P. Gaikwad, V. Samuel, V. Ravi, Bull. Mater. Sci. 27 (2004) 221–222.
[14] A.E. Kandjani, P. Salehpoor, M.F. Tabriz, N.A. Arefian, M.R. Vaezi, Mater. Sci.-Poland 28 (2010) 377–391.
[15] A.L. Linsebigler, G. Lu, J.T. Yates, Chem. Rev. 95 (1995) 735–758.
[16] V. Augugliaro, M. Litter, L. Palmisano, J. Sori, J. Photochem. Photobiol. C 7 (2006) 127–144.
[17] L.F. Liotta, M. Gruttadauria, G. Di Carlo, G. Perrini, V. Librando, J. Hazard. Mater. 162 (2009) 588–606.
[18] H. Xia, H. Zhuang, T. Zhang, D. Xiao, Mater. Lett. 62 (2008) 1126–1128.
[19] T.Y. Wei, C.Y. Kuo, Y.J. Hsu, S.Y. Lu, Y.C. Chang, Microporous Mesoporous Mater. 112 (2008) 580–588.
[20] Z. Wang, B. Yang, Z. Fu, W. Dong, Y. Yang, W. Liu, Appl. Phys. A 81 (2005) 691–694.
[21] M. Rezaei, S.M. Alavi, S. Sahebdelfar, Yan Zi-Feng, H. Teunissen, J.H. Jacobsen, J. Sehested, J. Mater. Sci. 42 (2007) 1228–1237.
[22] H.R. Pouretedal, M. Hosseini, Acta Chim. Slov. 57 (2010) 415–423.
[23] H.R. Pouretedal, A. Kadkhodie, Chin. J. Catal. 31 (2010) 1328–1334.
[24] H.Y. Chang, H.I. Chen, J. Cryst. Growth 283 (2005) 457–468.
[25] J. Xu, G. Li, L. Li, Mater. Res. Bull. 43 (2008) 990–995.
[26] Y. He, B. Yang, G. Cheng, Catal. Today 98 (2004) 595–600.
[27] J.A. Lewis, J. Am. Ceram. Soc. 83 (2000) 2341–2359.
[28] S.K. Pardeshi, A.B. Patil, Sol. Energy 82 (2008) 700–705.
[29] A. Nezamzadeh-Ejhieh, Z. Salimi, Appl. Catal. A 390 (2010) 110–118.
[30] A. Nezamzadeh-Ejhieh, S. Hushmandrad, Appl. Catal. A 388 (2010) 149–159.
[31] H.R. Pouretedal, M.H. Keshavarz, J. Alloys Compd. 501 (2010) 130–135.
[32] L. Jiang, G. Sun, Z. Zhou, S. Sun, Q. Wang, S. Yan, H. Li, J. Tian, J. Guo, B. Zhou, Q. Xin, J. Phys. Chem. B 109 (2005) 8774–8778.
[33] N. Daneshvar, S. Aber, M.S. Seyed Dorraji, A.R. Khataee, M.H. Rasoulifard, Int. J. Chem. Biomol. Eng. 4 (2008) 24–29.
[34] S.K. Kansal, M. Singh, D. Sud, J. Hazard. Mater. 141 (2007) 581–590.